

# Photoionization models of roundish galactic planetary nebulae in the thick disk<sup>\*</sup>

M. Emprechtinger<sup>1</sup>, T. Rauch<sup>2,3</sup>, and S. Kimeswenger<sup>1</sup>

<sup>1</sup> Institut für Astrophysik der Universität Innsbruck, Technikerst. 25, A-6020 Innsbruck, Austria

<sup>2</sup> Dr.-Remeis-Sternwarte, Sternwartstraße 7, D-96049 Bamberg, Germany

<sup>3</sup> Institut für Astronomie und Astrophysik, Abteilung Astronomie, Sand 1, D-72076 Tübingen, Germany

Received / accepted

**Abstract.** We present the result of photo-ionizing modelling of the three planetary nebulae (PNe) A 20, A 15 and MeWe 1-3. All three objects are roughly roundish, highly excited and have a high galactic  $z$ . The PNe displayed low densities in the shell, but relatively dense halos. A low metallicity and a relative high electron temperature were found. Comparisons with radio observations confirmed the obtained properties. The objects are very likely originating from thick disk stellar progenitors. The distances found investigating the PNe shells are somewhat lower than those derived spectroscopically with the central stars in the past.

**Key words.** planetary nebulae: individual: A 20, A 15, MeWe 1-3

## 1. Introduction

Although the interacting wind model for the formation of planetary nebulae (PNe) is accepted since a long time (Kwok et al. 1978), the exact mechanism is not clearly understood up to now. Several numerical simulations have been carried out especially during the last decade (e.g. Frank & Mellema (1994a), Dwarkadas & Balick (1998) or Schönberner & Steffen (2002)). The last one carried out an one-dimensional hydrodynamic simulation based on the evolutionary tracks of Blöcker (1995) and the simulations of the circumstellar shell around Asymptotic Giant Branch (AGB) star (Steffen et al. 1998).

The results of their simulation showed that a shock-bounded ionized main PN shell moving supersonically into the AGB-material compressing the inner parts of the matter into a dense but thin shell. The unaffected AGB-material becomes ionized as well and forms a rapidly expanding halo. Due to the drop of luminosity of the central stars of the PNe (CSPN) towards the white dwarf regime the outer part of the PN shell recombines quickly forming an second inner halo. The disadvantage of this simulation is that it just considers one dimension. Thus more complex

interactions of the winds like Rayleigh-Taylor instabilities, quickly building a clumpy environment as we see it in HST images, are not taken into account. This causes that the filling factor ( $\epsilon$ ) was set in fact to unity. Comparing densities obtain from forbidden line ratios and the one obtained from radio data or similar methods clearly show a filling factor far below unity (e.g. Mallik & Peimbert 1988 and Boffi & Stanghellini 1994). This changes the dramatically the optical thickness for ionizing UV photons and thus a recombining PN-shell is doubtful (Armsdorfer et al. 2002). The three PNe A 20, A 15 (Abell 1955) and MeWe 1-3 (Melmer & Weinberger 1990) were selected as they are roughly roundish objects. The central stars of the PNe (CSPNe) are well studied spectroscopically (Rauch et al. 1999, McCarthy et al. 1997, Saurer et al. 1997). This allows us to fix the input of radiation for the nebula. We modelled the physical properties of PNe-shells of three objects and compare the results with the theory.

## 2. Input Data

### 2.1. Observations and Data Reduction

Most data were obtained 1992 January 29<sup>th</sup> and January 30<sup>th</sup> using the New Technology Telescope (NTT) with the EMMI spectrograph at ESO La Silla, Chile and were taken from the ESO data archive. THX31156 (red arm) or TK1024AF (blue arm) CCDs and grating #8 were used. The slit-width was adjusted to 1''2. The spatial resolution was 0''44 per pixel at the red arm of the instrument (480

Send offprint requests to: M. Emprechtinger,  
e-mail: martin.emprechtinger@uibk.ac.at

<sup>\*</sup> Based on observations collected at the European Southern Observatory, La Silla under prog-id. 56.D-0717 and on observations made with the European Southern Observatory telescopes obtained from the ESO/ST-ECF Science Archive Facility.

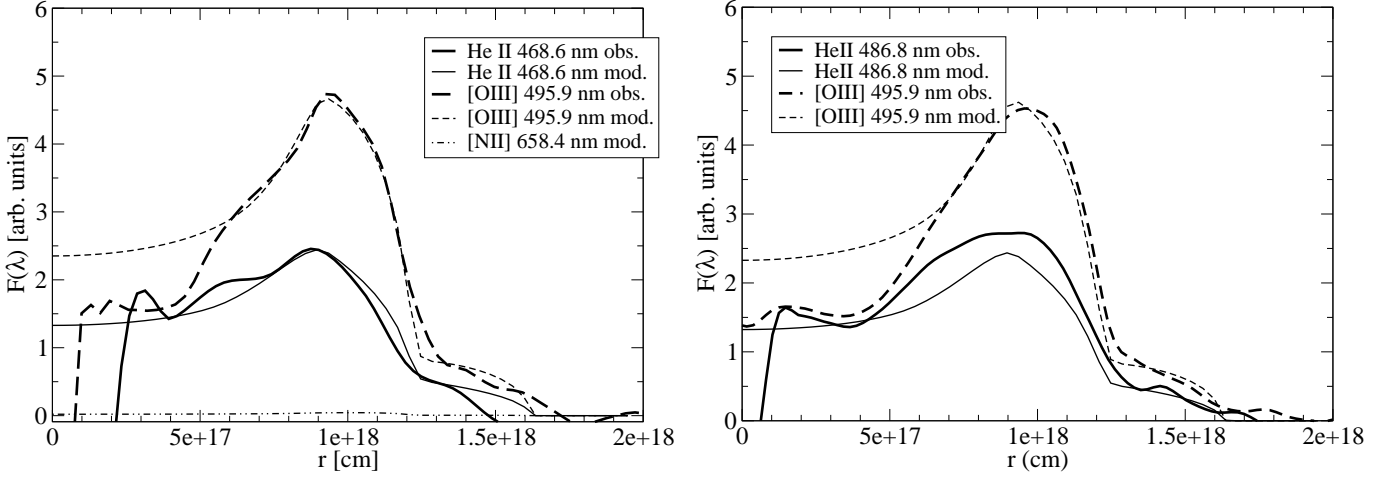


**Fig. 1.** The observations and the model for several lines of A 20. **Left:** Observation with NTT/EMMI (slit N–S); **Right:** Observation with ESO 3.6 m/EFOSC (slit E–W); especially in the [O III] lines the radial symmetry of the object is well pronounced. Also the fragmentation in three parts, halo, PN shell and central cavity, is displayed well. The [N II] lines are in an upper limit and thus confirm clearly the low metallicity found here (see Tab. 5).

nm to 680 nm) and  $0''.37$  at the blue arm (400 nm to 505 nm). Additionally A 20 was observed by one of us (TR) in 1996 February 10<sup>th</sup> with the ESO 3.60 m telescope using the EFOSC1 spectrograph and the #26 TEK512M 1215-3 detector at a resolution of  $0''.61$  per pixel (from 380 nm to 530 nm). At EFOSC observations narrow band [O III] and  $H\alpha$  images was taken too.

The calibration was done using usual procedure in MIDAS and the calibration data from EMMI manual and from EFOSC1 manual. The standard star EG 21 (Hamuy et al. 1992) was used for flux calibration.

The target selection for this investigation followed two criteria: First, the PN should have a roughly round shape; second, the CSPN should be spectroscopically studied.

**Table 1.** Basic data for the PNe sample:

Name	GPN (Kimeswenger 2001)	$F_{1.4 \text{ GHz}}$ [mJy]	IRAS
A 20	G214.96+07.81	10.4	07203+0151
A 15	G233.53–16.31	< 2.5	06249–2520
MeWe 1–3	G308.26+07.79	-	13249–5426

For all three objects IRAS counterparts have been found and radio-observations at 1.4 GHz have been found for two of them (Condon & Kaplan 1998). The objects are summarized in Tab. 1.

## 2.2. Spectroscopy

All three objects are characterized by an intensive He II line ( $\lambda = 468.3$  nm) and a total depletion of [N II] and [S II] lines. The [O III] lines at  $\lambda = 495.9$  nm and  $\lambda = 500.7$  nm are much weaker than expected as well. The extinction was derived from the Balmer-decrement and to deredden the

**Table 2.** Interstellar foreground extinction from the Balmer decrement derived here and from literature:

Name	E(B–V) here	E(B–V) Tylanda et al. (1992)
A 15	$0^m00$	$0^m04 - 0^m64$
A 20	$0^m05$	$0^m30 - 0^m35$
MeWe 1–3	$0^m27$	—

frames we used the interstellar extinction law by Savage & Mathis (1979). The results are given in Tab. 2. For A15 and A20 our results from the Balmer-decrement of the high S/N spectra differ significantly from those derived from the survey spectra in Tylanda et al. (1992). After dereddening with our values from Tab. 2 the continuum of the CSPN fits perfectly to our results. Also the  $B - V$  of the CSPN from literature supports our results. The resulting  $(B - V)_0$  is then always between  $-0^m34$  and  $-0^m25$ . This is expected for the hot CSPNe. The relative errors of the line ratios were estimated by the variations of the ratios of  $H\alpha/H\beta$  and  $[O III]_{500.7}/[O III]_{495.9}$  along the radius. A conservative estimation gives an error of 10-15% for the relative line strength. Since the three [O III] lines at  $\lambda = 500.7$  nm,  $\lambda = 495.9$  nm &  $\lambda = 436.3$  nm are detected a temperature determination was possible (Tab. 3). The error of the ratio of [O III] lines was assumed to be 50 %, because the  $[O III]_{436.3}$  was very faint. Hence the accuracy of  $T_e$  was about  $T_{-3000}^{+11000}$  K. Although the error of  $T_e$  is relative high it turned out, that the electron temperature is significantly higher than the 10 000 K, typical for PNe. This is a signature of the low metallicity (see below), causing the cooling by forbidden lines to fail.

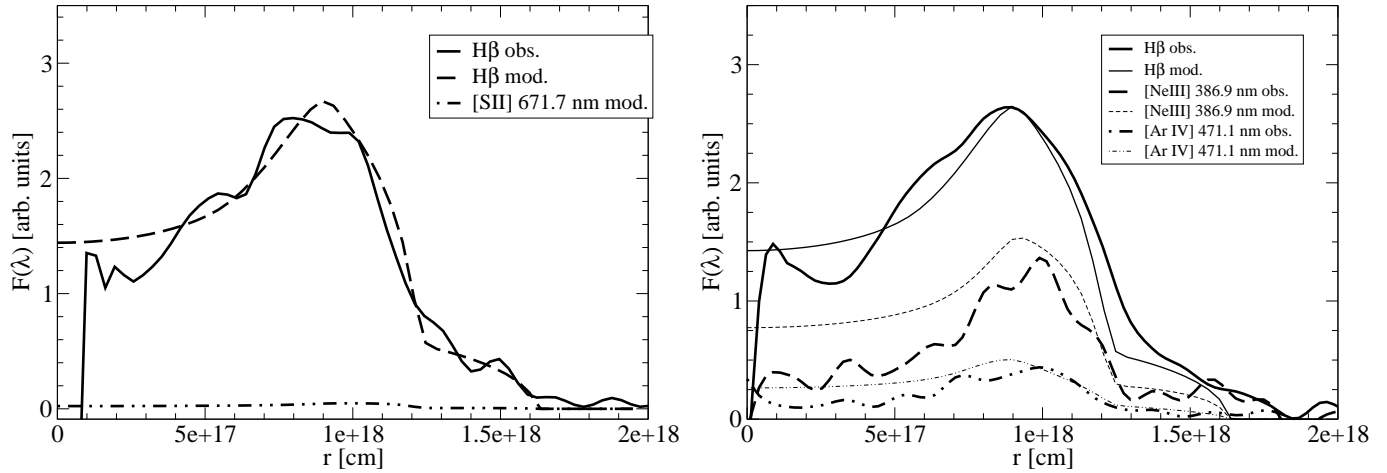


**Fig. 2.** Comparison of the observation and the model of several lines of A 20 (same as in Fig. 1).

**Table 3.** Electron temperatures derived from [OIII] lines and computed in CLOUDY:

Name	$\frac{I_{495.9} + I_{500.7}}{I_{436.3}}$	$T_e [K]$	$\langle T_e^{CLOUDY} \rangle [K]$
A 15	54.7	$16\,800^{+11\,000}_{-3\,000}$	23 000
A 20	71.5	$14\,800^{+11\,000}_{-3\,000}$	20 000
MeWe 1-3	62.2	$15\,800^{+11\,000}_{-3\,000}$	22 500

### 2.3. Central stars

The central stars of the objects have been studied very well in the past. Detailed spectroscopies were carried out by Rauch et al. (1999) (A 20), McCarthy et al. (1997) (A 15) and Saurer et al. (1997) (MeWe 1-3). To determine distances  $D_{CSPN}$  the method of Heber et al. (1984) was used for A 20 and A 15 in the papers above. In the case of MeWe 1-3 no distance was published before. We thus did it using an Eddington flux  $H_\nu$  given by Rauch (2004) following the method of Heber et al. (1984), who gave calibrations for Johnson and Stroemgren filters.

**Table 4.**

Name	$T_{\text{eff}}$ [kK]	$L$ [ $L_\odot$ ]	$\log g$ [ $\text{cm/s}^2$ ]	$D_{CSPN}$ [kpc]
A 20	$119 \pm 22$	2100	6.13	$4.1 \pm 50\%$
A 15	$110 \pm 10$	4238	5.7	$4.5 \pm 25\%$
MeWe 1-3	$100 \pm 10$	4580	5.5	$6.9 \pm 50\%$

Unfortunately no reliable photometry is available for the CSPNe of A 20 and MeWe 1-3, thus the error is considerably higher. But also for A 15 an error of 25 % was assumed according Mendez et al. (1988).

## 3. Photoionisation Model

To model the PNe the CLOUDY code (Ferland 1996) was used. As input-parameters the radial density-profile, the

chemical abundances and the stellar properties (within the ranges of error given above) were varied. The filling factor was assumed to be 0.1, which is typical for evolved PNe (Mallik & Peimbert (1988) and Boffi & Stanghellini (1994)). The NLTE central star models of Rauch (1997, 2003) were used to obtain a proper ionizing spectrum. Armsdorfer et al. (2002) showed the need of real NLTE stellar atmospheres to describe especially the HeII lines properly.

This results in the fraction of ionization of hydrogen and helium as a function of radius and a mean electron temperature. To obtain the surface-brightness, integration over the emissivity along the line of sight was carried out. To do this a spherical symmetry was adopted, what is indicated by round shape of the objects (see Soker (1997) and Tylanda et al. (2003) for A 20 and A 15). The surface-brightness of various emission lines have been compared with the observation to achieve the best result. The average electron temperature given by CLOUDY was compared with those derived before by the [OIII] lines. Due to the weak 436.3 nm line a spatial resolved study wasn't possible here.

The objects A 15 and MeWe 1-3 displayed enhancements in the southern regions, especially in [OIII]. This might be due to interaction with the interstellar medium. Thus this regions were not taken into account for the model.

### 3.1. A 20 (GPN G214.96+07.81)

A 20 is the only one of these objects that is observed with both telescopes, NTT and ESO 3.60 m. The advantage of the doubled observation is that the slit direction was north-south at NTT and east-west at the ESO 3.60 m telescope and thus we were able to rule out systematic effects in the data reduction and due to the assumed spherical symmetry.

In Fig. 1 & 2 the result of the modelling can be seen. The model was optimized with respect to the NTT spectra. In the east-west direction the HeII line is slightly stronger

than in north-south but both observed spectra agree fairly well with the model. Just in the very inner part the model displays an emissivity, especially of the [OIII] line, that is too high compared with the observations. This deficiency is, although uncertain, most likely originating in deviations from the spherical symmetry assumed in the CLOUDY code. The modelled [SII] and [NII] lines are far below the limit of detection and thus confirmed by the observation. EFOSC-images do not display the regime, where the [NII] and [SII] lines are located, but the line of [NeIII] at  $\lambda = 386.9$  nm and of [ArIV] at  $\lambda = 471.1$  nm. The [ArIV] line is very faint and the [NeIII] at the blue limit of the spectrograph, where the efficiency of the CCD and the transparency of the spectrograph have not good performances. Thus their error is higher than the one of the other lines.

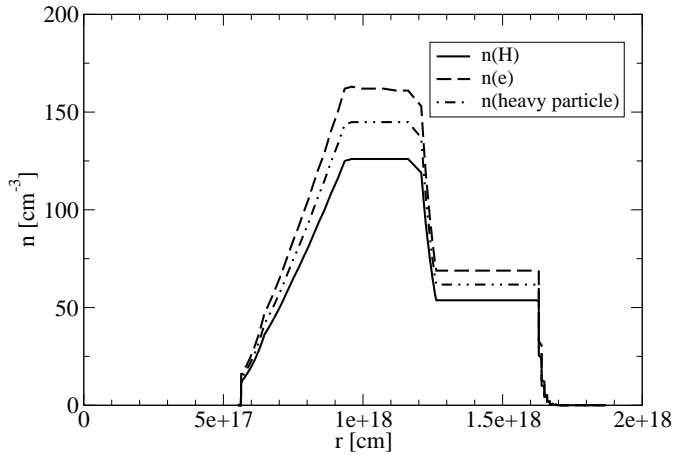


**Fig. 3.** Density profile of A 20. The hydrogen- and the electron density are computed by CLOUDY. The heavy particle density is calculated from the hydrogen density and the chemical composition.

In Fig. 3 the density profile of A 20 can be seen. The heavy particle density is mostly hydrogen and helium. Other elements contribute less than  $2 \cdot 10^{-4}$ . The high electron density, which exceeds the hydrogen density twice as much as the heavy particle density, indicates a mostly doubly ionized helium, what is confirmed in Fig. 4.

The chemical composition (Tab. 5) shows clearly an underabundance of heavy elements by a factor of 10. This makes it most likely to a member of the galactic thick disk population. The total depletion of [SII] and [NII] lines can be explain just partial by the underabundance of these elements. It is also caused by the fact that these elements are mainly in a higher ionization level. The overabundance of He is typical for PNe after the dredge-up processes during the RGB/AGB phase.

The halo of the nebula is clearly highly ionized. It is not a recombination halo as predicted by 1D hydro simulations.

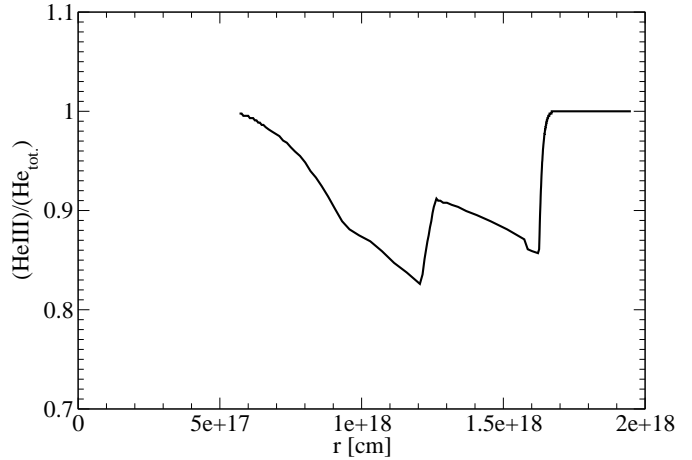


**Fig. 4.** The fraction of doubly ionized helium as a function of radius. As can be seen helium is mostly doubly ionized, as it was expected considering the high HeII 468.6 nm intensity.

**Table 5.** Chemical composition of A 20. The abundances of each element  $Z$  are given in  $\log \frac{[Z]}{[H]}$  and the comparison with the solar abundances (Grevesse et al. 1996) is given in *dex*.

	abundance	abundance compared to solar abundance	dominating ionization level
He	-0.825	0.175	He III
C	-4.45	-1.00	C IV
N	-5.00	-0.97	N IV
O	-4.10	-0.97	O IV
Ne	-4.824	-0.90	Ne IV
Mg	-5.523	-1.10	Mg III
Si	-5.523	-1.07	Si III
S	-5.824	-1.15	S IV
Ar	-5.80	-0.32	Ar IV

### 3.2. A 15 (GPN G233.53–16.31)

In Fig. 5 the surface brightness distributions for several lines of A 15 are displayed. There is hardly any decrease of the intensity towards the center of the nebula, contrary to A 20. This indicates that the inner part of the nebula is not empty, like in A 20, but somehow filled as can be seen in Fig. 6. The intensity of [SII] and [NII] is again, in conformity with the observations, below the threshold of detection. Also here the HeII line looks like the H $\beta$ . Another remarkable fact is, that the [OIII] is less prominent than the H $\beta$  and the HeII line.

In the inner part of the nebula the density relates to the radius as  $r^{-0.3}$ . The main shell is thinner and has a lower density than the one of A 20 and followed by a relative extended and dense halo. The hydrogen in A 15 is also totally ionized as well as most of the helium (Fig. 6).

The fraction of heavy elements is in this object even slightly lower than in A 20 and the electron temperature thus is higher as the cooling by the forbidden lines fails (see Tab. 3 what still agrees with the  $T_e=23000$ K com-

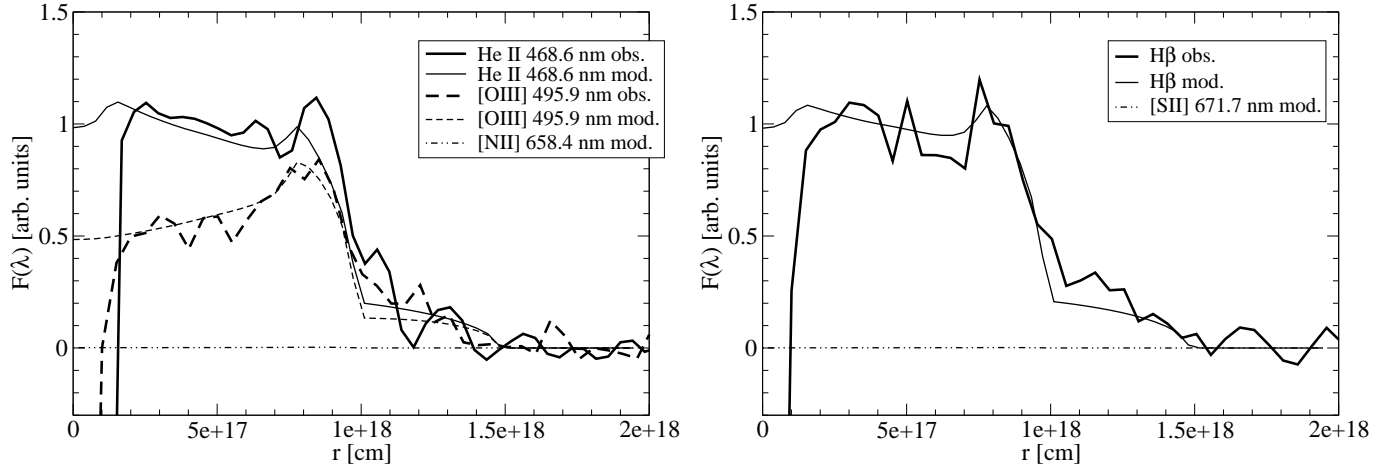


**Fig. 5.** Comparison of the observation and the model of several lines of A 15.  $H\alpha$  and [OIII] ( $\lambda = 500.7$  nm) are not taken into account since they are related to  $H\beta$  and [OIII] ( $\lambda = 495.9$  nm) respectively. The [NII] and the [SII] was not observable. The innermost 'hole' in the data is faked due to the CSPN subtraction/overlay.

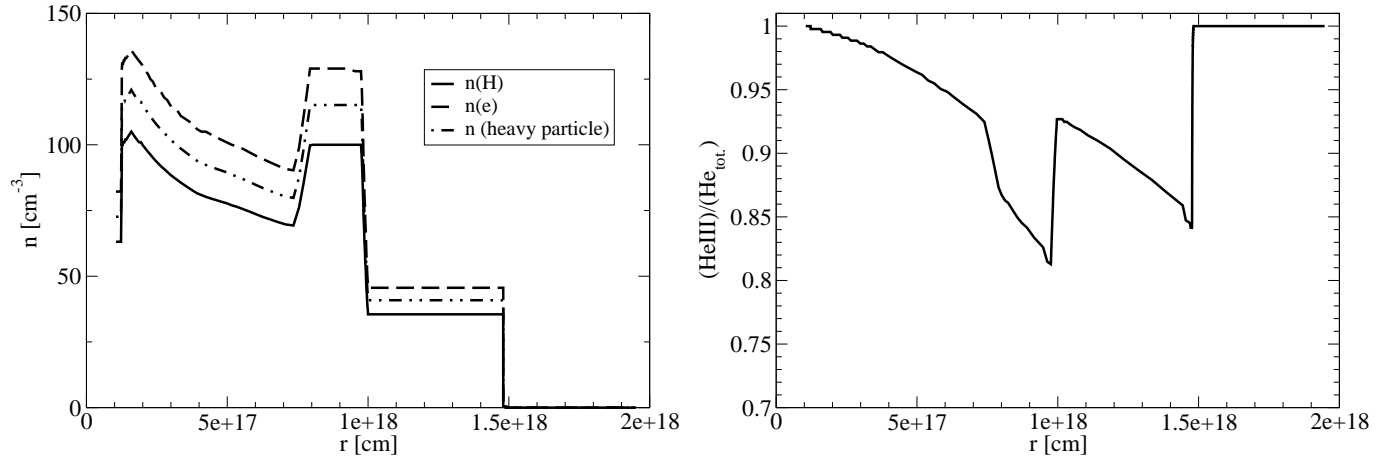


**Fig. 6.** Density profile and fraction of doubly ionized helium of A15. Description like in Fig. 3 & Fig. 4

puted by CLOUDY). Also the dominating ionization levels are slightly higher than the one in A 20, especially the one of C, S, and Si. The typical He enrichment is shown by A 15 too. The overabundance of nitrogen with respect to the other heavy elements give us not an hint for a massive progenitor, but originates in the upper limit of the observed line.

### 3.3. MeWe 1-3 (GPN G308.26+07.79)

MeWe 1-3 shows, even if it is not so pronounced like the one in A 20, an inner central cavity. Also in respect to other conditions it looks like A 20, as there are the similarity of the HeII and the  $H\beta$  line, the relative line strength of [OIII] and the lack of any [SII] and [NII] lines. Only there is hardly any halo visible in MeWe 1-3.

Since the emissivity distribution of MeWe 1-3 looks like the one of A 20 their density profile is similar – an empty inner part, and a rapid increase of the density to a plateau, here at  $100 \text{ H cm}^{-3}$ . Just the narrowness of the halo of only  $0.013 \text{ pc}$  is different. In this case the whole nebular

**Table 6.** Chemical composition of A 15 (same as in Tab. 5).

	abundance	abundance compared to solar abundance	dominating ionization level
He	-0.82	0.18	He III
C	-4.95	-1.50	C V
N	-5.03	-1.0	N IV
O	-4.60	-1.47	O IV
Ne	-5.420	-1.50	Ne IV
Mg	-5.920	-1.50	Mg III
Si	-5.950	-1.5	Si V
S	-6.17	-1.5	S V
Ar	-6.98	-1.5	Ar IV

hydrogen and helium is mostly bare of all electrons too. Also the abundances of the elements are very similar to the one of A 20. But the average ionization stage is closer to the one of A 15. Also the electron temperature ( $15\,800 \text{ K}$  observation,  $22\,500 \text{ K}$  model) is in between the two other nebulae, and that despite the lower  $T_{\text{eff}}$  of its central star.

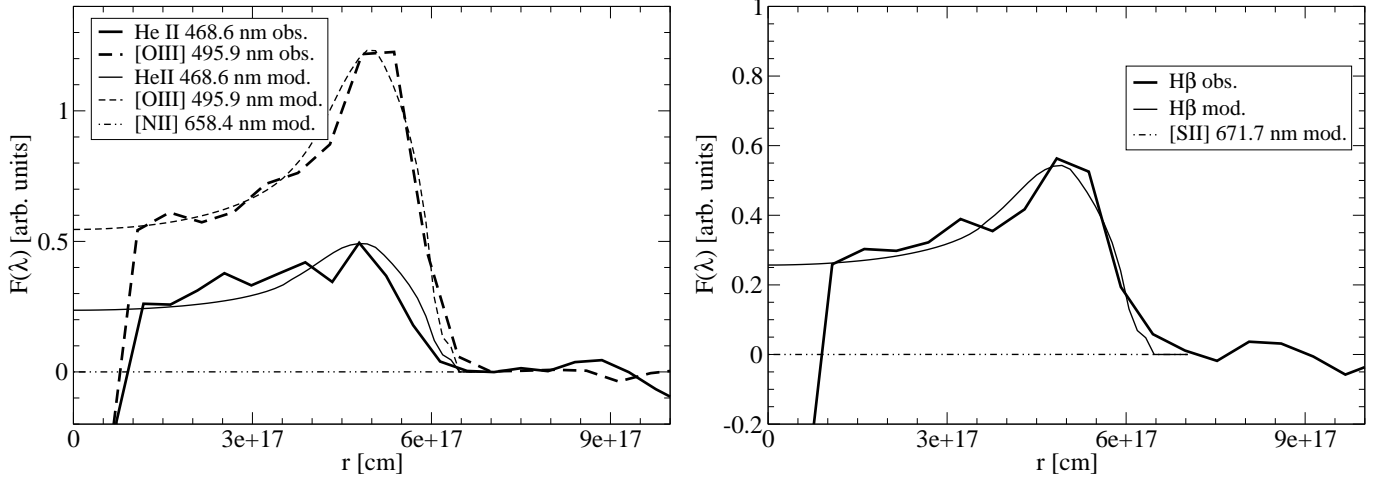


**Fig. 7.** Comparison of the observation and the model of several lines of MeWe 1-3 (description see Fig. 5).

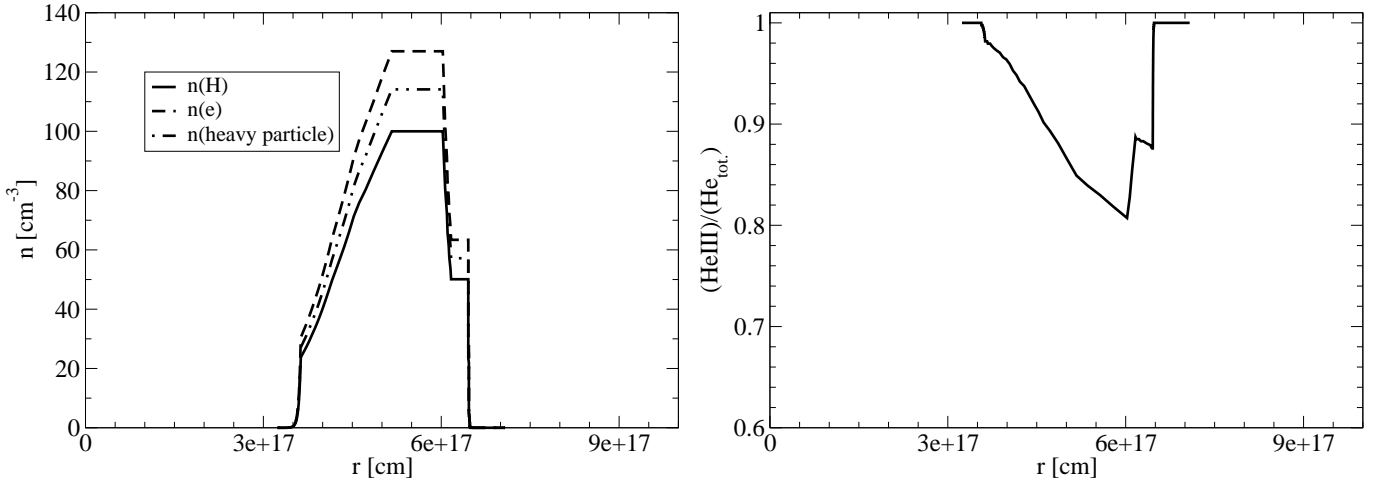


**Fig. 8.** Density profile (left) and fraction of doubly ionized helium of MeWe 1-3.

The larger luminosity of the CSPN of MeWe 1-3 and the smaller radius of the nebula itself is able explain this effect.

**Table 7.** Chemical composition of PN MeWe 1-3 (same as in Tab. 5).

	abundance	abundance compared to solar abundance	dominating ionization level
He	-0.85	0.15	He III
C	-4.45	-1.0	C IV
N	-5.03	-1.0	N IV
O	-4.13	-1.0	O IV
Ne	-5.03	-1.11	Ne IV
Mg	-5.42	-1.0	Mg III
Si	-5.45	-1.0	Si V
S	-5.67	-1.0	S V
Ar	-6.48	-1.0	Ar IV

Since the errors of the properties of the objects, given in the literature, are relatively large, especially for the

luminosity and the distance, we varied them within the ranges of error. The obtained data are given in Tab. 8.

**Table 8.** Obtained basic data of the PNe modeled.

Name	$T_{eff}$ [kK]	$L$ [ $L_{\odot}$ ]	radius [pc]	dist. [kpc]
A 20	140	3000	0.40	2.35
A 15	120	4200	0.32	4.01
MeWe 1-3	110	4500	0.21	3.95

It seems that the temperature and thus the luminosity of the CSPN of A 20 are underestimated. The uncertain distances of A 20 and MeWe 1-3 are always smaller in the models compared to the one given in the literature, but still within the error-deviation.

#### 4. Discussion and Conclusion

The metallicities of all three PNe investigated are lower by a factor of 10 to 30 compared to the solar abundances, only helium is little bit more present than in the Sun.

Soker (2002) already reports an under-abundance of metals in round PNe.

Looking at the galactic coordinates and the distances of the planetary nebulae one can easily verify that the height above the galactic plane ( $z$ ) of these nebulae is comparatively large (Fig. 9).

The nebulae investigated are located at a  $z$  of 320 pc, -1127 pc and 535 pc for A 20, A 15 and MeWe 1-3 respectively. To compare these values with other one the PNe catalogued by Acker et al. (1992) were taken as a representative sample for all PNe. Half of these planetary nebulae are located below a  $z$  of 162 pc. Their average  $z$  amounts to 288 pc. The large  $z$  of the three objects investigated indicates that they are so called thick disk objects and therefore their progenitor was an underabundant object as well.

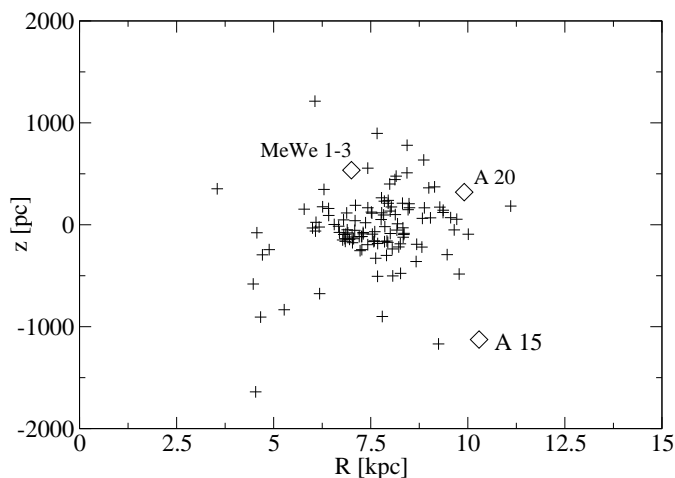


**Fig. 9.** Here the galactic height  $z$  versus the radius from the galactic center is displayed. The radius of the sun was assumed to be 8 kpc. The + shows the PNe catalogued by Acker et al. (1992) and the  $\diamond$  the PNe A 20, A 15 and MeWe 1-3.

The high electron temperature of the nebulae is also linked to the low metallicity (Stasinska (1978)). As Frank & Mellema (1994b) showed one important cooling mechanisms in ionized gas is the radiation emitted by collisionally excited lines. The most important role plays the [NII] lines in low excited nebulae and the [OIII] lines in high excited one. Since no [NII]- and less intensive [OIII] lines, compared to common PNe, are detected a higher temperature is feasible.

As mentioned above a filling factor ( $\epsilon$ ) of 0.1 was adopted. Since radio data are available for A 20 and A 15 (Condon & Kaplan 1998) it was possible to check this assumption. Adopting a optically thin wind in the radio regime and therefore  $I_\nu \propto \nu^{-0.1}$  allows us to compute the radio flux at 5 GHz from the 1.4 GHz data and thus the total ionized mass according Cahn et al. (1992).

$$M_{\text{ion.}} = \sqrt{2.266 \times 10^{-21} \cdot D^5 \cdot \theta^3 \cdot F_{5 \text{ GHz}}}$$

where  $D$  is the distance in pc,  $\theta$  the angular radius in arcseconds and  $F_{5 \text{ GHz}}$  the radio flux at 5 GHz in Jansky. We compared this mass with the one of our model, computed by

$$M = 4\pi\mu \int_0^{+\infty} n_{\text{hp}}(r)r^2 dr$$

$\mu$  is the mean atomic weight and  $n_{\text{hp}}(r)$  the heavy particle density as function of the radius. This results in  $\epsilon$ . Although the error of the obtained filling factor is quiet high it is clearly smaller than 0.3. Using the sample and the formula of Mallik & Peimbert (1988) we obtain a value even below 0.05. The formula of Boffi & Stanghellini (1994) give a value of 0.096. But especially the sample shows no PN with a radius above 0.2 pc and an filling factor above 0.1. Tests with CLOUDY show that the nebulae are always optically thin for the UV radiation up to  $\epsilon = 0.5$ .

Further calculations showed that even stars with luminosities down to  $160 L_\odot$  are able to ionize most of the hydrogen and thus a recombination of the shell seems to be impossible. This is in clear contradiction to the predictions of the 1D hydro simulations (e.g. Schönberner & Steffen 2002).

While the luminosities of the CSPN found from the investigation of the PN shells here are about the same as those found with the NLTE models of the CSPN spectroscopy. Our temperatures are - still within the error bars - slightly higher than those from the CSPN spectra. As shown by Lechner & Kimeswenger (2004) and Emprechtinger et al. (2004) these parameters are very sensitive to the line ratios of the highly ionized species. We thus suggest this effect to be real. The distances  $D_{\text{CSPN}}$  have to be significantly lower than those found by other investigations in the past.

*Acknowledgements.* This research was supported by the DLR under grant 50 OR.0201 (TR). We thank the referee R. Szczerba for the valuable comments improving the original manuscript.

## References

- Abell, G.O., 1955, PASP, 67, 258
- Acker, A., Ochsenbein, F., Stenholm B. et al., 1992, Strasbourg-ESO Catalogue of Planetary Nebulae
- Armsdorfer, B., Kimeswenger, S., & Rauch, T. 2002, RevMexAA (Serie de Conf.), 12, 180
- Blöcker, T., 1995, A&A, 299, 755
- Boffi, F.R., & Stanghellini, L., 1994, A&A, 284, 248
- Cahn, J.H., Kaler, J.B., & Stanghellini, L., 1992, A&AS, 94, 399
- Condon, J.J., & Kaplan, D.L., 1998, ApJS, 117, 361
- Dwarkadas, V., & Balick, B., 1998, ApJ, 497, 267
- Emprechtinger, M., Forveille, T., & Kimeswenger, S. 2004, A&A, 423, 1017
- Ferland, G., 1996, A Brief Introduction to Cloudy 90.05, Univ. Kentucky, Department of Physics and Astronomy, Internal Report
- Frank, A., & Mellema, G., 1994a, ApJ, 430, 800

- Frank, A., & Mellema, G., 1994b, *A&A*, 289, 937
- Grevesse, N., Noels, A., & Sauval, A.J. 1996, *ASP Conf. Ser.*, 99, 117
- Hamuy, M., Walker, A.R., Suntzeff, N.B. et al., 1992, *PASP* 106,566
- Heber, U., Hunger, K., Jonas, G., & Kudritzki, R. P., 1984, *A&A*, 130, 119
- Kimeswenger, S. 2001, *Rev. Mex. A&A*, 37, 115
- Kwok, S., Purton, C.R., & Fitzgerald, P.M., 1978, *ApJ*, 219, 125
- Lechner, M.F.M., & Kimeswenger, S. 2004, *A&A* in press (astro-ph/0406507)
- Mallik, D.C.V., & Peimbert, M., 1988, *RMxAA*, 16, 111
- McCarthy, J.K., Mendez, R.H., & Kudritzki, R.P., 1997, *IAUS*, 180, 120
- Melmer, D., & Weinberger, R., 1990, *MNRAS*, 243, 236
- Mendez, R.H., Kudritzki, R.P., Herrero, A., Husfeld, D., & Groth, H.G., 1988, *A&A*, 190, 113
- Rauch, T., 1997, *A&A*, 320, 237
- Rauch, T., 2003, *A&A*, 403, 709
- Rauch, T., 2004, <http://astro.uni-tuebingen.de/~rauch/>
- Rauch, T., Köppen, J., Napiwotzki, R., & Werner, K., 1999, *A&A*, 347, 169
- Saurer, W., Werner, K., & Weinberger, R., 1997, *A&A*, 328, 598
- Savage, B.D., & Mathis, J.S., 1979, *ARA&A* 17, 73
- Schönberner, D., & Steffen, M., 2002, *RMxAC*, 12, 144
- Soker, N., 1997, *ApJS*, 112, 487
- Soker, N., 2002, *A&A*, 386, 885
- Stasinska, G., 1978, *A&AS*, 32, 429
- Steffen, M., Szczerba, R., & Schönberner, D., 1998, *A&A*, 337, 149
- Tylenda, R., Acker, A., Stenholm, B., & Koeppen, J., 1992, *A&AS*, 95, 337
- Tylenda, R., Sidmiak, N., Gorny, S. K., Corradi, R. L. M., & Schwarz, H. E., 2003, *A&A*, 405, 627